

# Chemical Science

Accepted Manuscript



This is an *Accepted Manuscript*, which has been through the Royal Society of Chemistry peer review process and has been accepted for publication.

*Accepted Manuscripts* are published online shortly after acceptance, before technical editing, formatting and proof reading. Using this free service, authors can make their results available to the community, in citable form, before we publish the edited article. We will replace this *Accepted Manuscript* with the edited and formatted *Advance Article* as soon as it is available.

You can find more information about *Accepted Manuscripts* in the [Information for Authors](#).

Please note that technical editing may introduce minor changes to the text and/or graphics, which may alter content. The journal's standard [Terms & Conditions](#) and the [Ethical guidelines](#) still apply. In no event shall the Royal Society of Chemistry be held responsible for any errors or omissions in this *Accepted Manuscript* or any consequences arising from the use of any information it contains.

## ARTICLE

# Mapping the Electrogenenerated Chemiluminescence Reactivity in Space: Mechanistic Insight into Model Systems Used in Immunoassays

Cite this: DOI: 10.1039/x0xx00000x

Received 00th January 2012,  
Accepted 00th January 2012

DOI: 10.1039/x0xx00000x

www.rsc.org/

Milica Sentic,<sup>a,b</sup> Milena Milutinovic,<sup>a,b</sup> Frédéric Kanoufi,<sup>c</sup> Dragan Manojlovic,<sup>b</sup> Stéphane Arbault<sup>a</sup> and Neso Sojic<sup>a</sup>

The remarkable characteristics of electrogenerated chemiluminescence (ECL) as a readout method are successfully exploited in numerous microbead-based immunoassays. However there is still a lack of understanding of the extremely high sensitivity of such ECL bioassays. Here the mechanisms of reaction between the  $\text{Ru}(\text{bpy})_3^{2+}$  luminophore with two efficient co-reactants (TPrA or DBAE) were investigated by mapping the ECL reactivity at the level of single  $\text{Ru}(\text{bpy})_3^{2+}$ -functionalized beads. Micrometric non-conductive beads were decorated with the ruthenium label *via* a sandwich immunoassay or *via* a peptidic bond. Mapping the ECL reactivity on one bead demonstrates the generation of the excited state at micrometric distance from the electrode by reaction of surface-confined  $\text{Ru}(\text{bpy})_3^{2+}$  with diffusing TPrA radicals. The signature of the  $\text{TPrA}^{\bullet+}$  lifetime is obtained from the ECL profile. Unlike with  $\text{Ru}(\text{bpy})_3^{2+}$  solution, DBAE generates very low ECL intensity in the bead-based format suggesting more instable radical intermediates. The 3D imaging approach provides insights into the ECL mechanistic route operating in bioassays and on the optical effects to focus the ECL signal.

## Introduction

Electrogenenerated chemiluminescence (ECL) is the process of light emission by the excited state of a luminophore upon electrochemical stimulation.<sup>1</sup> Species generated at an electrode undergo high-energy electron-transfer reactions to give excited states. The discovery of ECL emission in aqueous media has led to important bioanalytical applications including clinical diagnostics.<sup>2, 3</sup> The process is based on a reaction cascade initiated at an electrode surface between a sacrificial co-reactant species and a luminophore. Model systems providing high ECL efficiency consist of the luminophore  $\text{Ru}(\text{bpy})_3^{2+}$  with either tri-*n*-propylamine (TPrA)<sup>4-6</sup> or 2-(dibutylamino)ethanol (DBAE)<sup>7</sup> as co-reactants. ECL mechanism of the tandem  $\text{Ru}(\text{bpy})_3^{2+}$ /TPrA system is an active area of investigation and there is still a lack of understanding of the extremely high sensitivity of the bioassays using ECL as a readout method.<sup>8-10</sup> Bead-based ECL assays have been the object of numerous works and they are currently commercialized for a large number of immunoassays, such as for cardiac and infectious diseases, thyroid, tumour markers, *etc.*<sup>3, 11-17</sup> In such assays, beads are functionalized with a specific antibody to capture analyte molecules in a sample. As in the present report, a sandwich immunoassay is performed by exposing the beads to a detection antibody conjugated to a  $\text{Ru}(\text{bpy})_3^{2+}$  label (Figure 1a), collecting them onto an electrode and finally generating ECL in the presence of TPrA.

Different competitive mechanistic pathways have been proposed to explain the ECL emission of the  $\text{Ru}(\text{bpy})_3^{2+}$ /TPrA system.<sup>3</sup> They

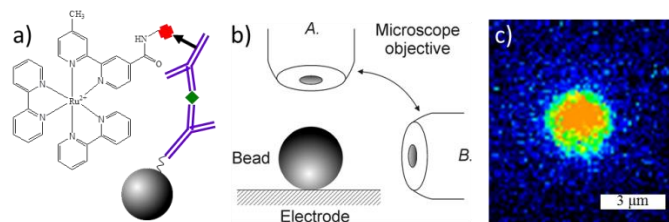


Fig. 1. (a) Sandwich immunoassay with PS beads. (b) Schematic representation of both optical configurations used to image the functionalized bead: top-view (A) and side-view (B). (c) ECL imaging of a single 3-µm bead using the top-view configuration. ECL images were acquired over a 6 s exposure-time at a potential of 1.1 V vs Ag/AgCl/KCl in a PBS solution containing 100 mM TPrA (pH = 7.4).

can be classified into two main groups depending on how  $\text{Ru}(\text{bpy})_3^{2+}$  is oxidized. The first one requires explicitly the direct oxidation of  $\text{Ru}(\text{bpy})_3^{2+}$  at the electrode surface to generate *in fine* the ECL emission. However, these mechanistic routes cannot account for the ECL features reported at low oxidation potentials and also for the excellent sensitivity of the bead-based immunoassays.<sup>8, 18</sup> In this case, only the ruthenium labels located on the bead within electron tunnelling distance from the electrode surface would be directly oxidized, meaning that an infinitesimal fraction of labels would contribute to the ECL signal following these paths. A second “revisited” route involving the mediated oxidation of  $\text{Ru}(\text{bpy})_3^{2+}$  by the cation radical ( $\text{TPrA}^{\bullet+}$ ) has been proposed by Miao *et al.* to

explain how ruthenium centres located at micrometric distances from the electrode might generate ECL.<sup>19</sup> In this path, only the co-reactant TPrA is oxidized at the electrode and the resulting radicals, TPrA<sup>•+</sup> and TPrA<sup>•</sup>, play the central role in the ECL process. Both species diffuse over short distances and react with the luminophore to generate its excited state, making this route essential in bead-based ECL assays. Besides, DBAE is an environmentally friendly co-reactant which could be expanded to bioassays as it shows better performance than TPrA in ECL operated with Ru(bpy)<sub>3</sub><sup>2+</sup> solution (not immobilized as for bead-based assays).<sup>7, 20</sup> The competitive pathways involving cascade of reactions of short-lived radicals with different redox potentials and reactivity at the minute scale crystallize the kinetic complexity of the overall ECL process,<sup>21, 22</sup> which might be difficult to simulate accurately in solution phase or to anticipate in real practical cases.

This work aims at deciphering the ECL phenomena operating in bead-based ECL bioassays. For this purpose, it is essential to investigate the mechanisms of Ru(bpy)<sub>3</sub><sup>2+</sup>/co-reactant systems at the single bead level, with either TPrA or DBAE, by imaging the 3D distribution of ECL intensity. In this report, the ruthenium label was attached to micrometric beads *via* a sandwich immunoassay or *via* a peptidic bond. Immobilizing the luminophore species simplifies the mechanistic routes as it depends solely on the local concentration variations of the electrogenerated co-reactant intermediates around the bead. The Ru(bpy)<sub>3</sub><sup>2+</sup> centers are exposed to the concentration gradients of the electrogenerated radical species. As in planar read/write approaches,<sup>23-25</sup> the local reading of the sphere reactivity, revealed by ECL, allows the volume interrogation of the reactive species propagation. Investigating the 3D ECL patterns recorded on such beads provides a global description of the ECL phenomenon.

## Results and discussion

A sandwich ECL immunoassay was performed by exposing polystyrene (PS) 3- $\mu$ m beads modified with a capture antibody (anti-IL-8) to a sample containing the antigen and biotinylated detection antibodies. Finally the streptavidin-modified Ru(bpy)<sub>3</sub><sup>2+</sup>-label was attached (Figure 1a). The beads were let to deposit on a flat glassy carbon (GC) electrode and ECL was recorded with a microscope in a top-view configuration (Figure 1b). Figure 1c shows a single functionalized bead emitting ECL light when a sufficient anodic potential of 1.1 V is applied to the GC electrode in a TPrA solution. One can observe that the ECL light emerges from the entire bead and not only from the region where the bead is in contact with the surface. The ruthenium label is attached to the bead and only the co-reactant radicals resulting from the oxidation step at the electrode diffuse and react with the label to generate the excited state. ECL intensity is not homogeneously distributed over the bead; it appears more intense in the centre. However, such an image does not allow resolving sufficiently the distribution of the ECL intensity.

To improve the spatial resolution of the luminescence phenomenon and to obtain well-resolved ECL patterns, we used in further experiments 12- $\mu$ m diameter PS beads functionalized with the same ruthenium label by an amide-type reaction (Scheme S1). The photoluminescence (PL) image shows the location of a labelled PS bead (Figure 2a). The PL intensity which reflects the immobilized ruthenium sites was homogeneously distributed over the bead. By increasing progressively the applied potential from 0.7 V, where no ECL is generated, to 1.2 V, ECL intensity increased progressively with a maximum value obtained at 1.1 V (Figure S1a).<sup>19</sup> Similarly, we observed with a good spatial resolution that the entire beads emit ECL light with a brighter spot in their centre. In fact, they act as an efficient lens focusing the light at their centre.

Such a peculiar electromagnetic field distribution that emerges from a dielectric microsphere has been experimentally demonstrated.<sup>26, 27</sup> The light beam emerges from the microsphere with high intensity and low divergence. Such a focusing behaviour concentrates the analytical signal and contributes to the extremely good sensitivity of the bead-based ECL immunoassays.

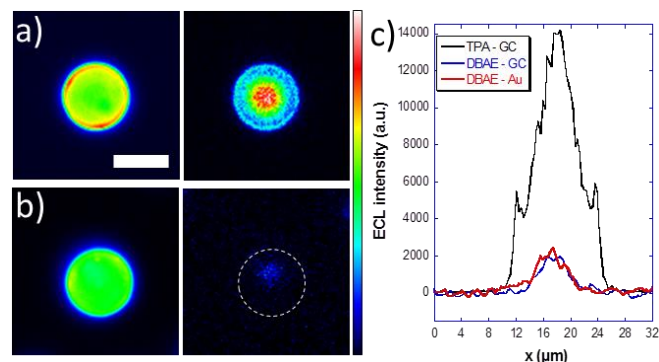


Fig. 2. (a-b) Top-view PL (left) and ECL (right) images of 12- $\mu$ m PS beads functionalized with the ruthenium label. ECL images were recorded in PBS solutions containing (a) 100 mM TPrA or (b) 20 mM DBAE on GC electrodes. The dashed line materializes the position of the bead. Experiments have been performed on more than 50 single beads in each condition. Scale bar: 10  $\mu$ m. (c) ECL intensity profiles taken along the middle vertical axis of the beads and recorded in 100 mM TPrA on GC electrode (black line) or in 20 mM DBAE on GC (red line) and on Au (blue line) electrodes.

Since DBAE has been reported to produce stronger ECL signal in solution than TPrA (e.g. 6.5-fold higher ECL signal at 20 mM co-reactant concentration),<sup>7</sup> we tested its performance in the bead-based format (Figure 2b). In our conditions, maximum ECL intensity has been obtained at 1.2 V with a DBAE concentration of 20 mM. ECL emission was located just at the centre of the bead over a  $\sim$ 4-5  $\mu$ m diameter surface (Figures S1b and 2c). Unexpectedly, the ECL intensity was extremely low on GC and on Au electrodes: ECL signals recorded on the functionalized beads were surprisingly 7-fold lower than those collected with TPrA. This difference may be explained by the different experimental conditions since, in previous reports,<sup>7, 20, 28</sup> Ru(bpy)<sub>3</sub><sup>2+</sup> was freely diffusing in solution and could react homogeneously with the DBAE radicals. In the bead-based format, radicals resulting from DBAE oxidation have to diffuse away from the electrode and to react with the immobilized Ru(bpy)<sub>3</sub><sup>2+</sup> to generate the excited state. Such behaviour highlights the difference in reactivity of both tested co-reactants which depends on the redox potentials and the lifetimes of their radicals. At first sight both the weaker and lesser expansion of ECL suggest that the DBAE-derived radicals propagate less in solution and are likely less stable than the TPA ones.

Even if the top-view imaging of the bead highlights the non-uniform distribution of ECL intensity over it, it does not give precise localization of the ECL-emitting region on its surface. Indeed, the recorded ECL pattern reflects mainly the optical paths through the beads. To reconstruct the spatial location and the volumic extension of the ECL-emitting zone, a 3D cartography, as in scintigraphy, can be obtained by changing the angle of observation of the emitting object. Here, we used an orthogonal side-view configuration (position B in Figure 1b). It supplements the top-view approach with a 2D ECL mapping normal to the electrode surface. Figure 3 shows the PL image of the bead: the upper part of the image corresponds to the real bead and the lower part to its mirror image formed by the light reflection on the GC surface. PL image precisely defines the

position of the bead and also its interface with the electrode. As for the top-view images, the ECL experiments with TPrA, did not show light emission before applying sufficiently anodic potentials (Figure 3). At 1.1 V, an ECL-emitting region was observed at the interface between the GC surface and the bead (*i.e.*  $z = 0$ ); this extends over a  $\sim 6 \mu\text{m}$  length knowing that this value integrates also the contribution of the light reflection. Interestingly, there is a second region from where ECL light emerged, located at the top of the PS bead. As discussed previously, it corresponds to the focusing effect of the bead which acts as a lens and does not contain any real chemical information. The ECL-emitting region was confined very close to the electrode surface and extended only over 3–4  $\mu\text{m}$  along  $z$  axis. With the side-view configuration, we were not able to record any ECL emission with DBAE even for exposure time of the CCD camera up to 20 s (Figure S2). Again, with DBAE, the extension of the ECL-emitting region is probably too small at the bead/electrode interface and its intensity too low to be imaged in our conditions.

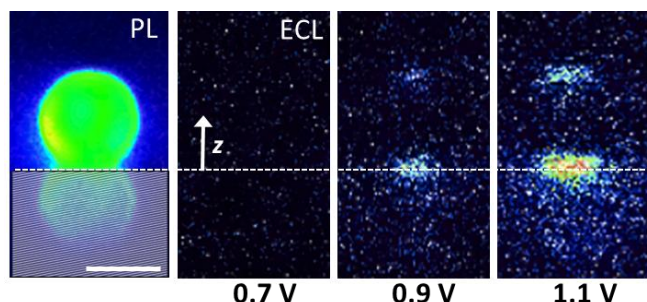
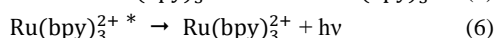
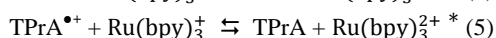
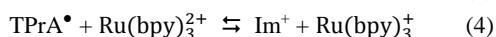
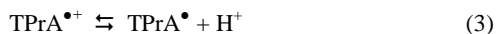


Fig. 3. Side-view images of a 12- $\mu\text{m}$  PS bead labelled with the ruthenium complex. The first image is obtained by PL and the following ones by ECL in a PBS solution containing 100 mM TPrA (pH = 7.4). The dashed line materializes the position of the GC electrode surface (*i.e.*  $z = 0$ ) and the hatched zone represents the PL reflection on the electrode surface. Same conditions as in Figure 1. Scale bar: 10  $\mu\text{m}$ .

The ECL mechanisms involving direct oxidation of  $\text{Ru}(\text{bpy})_3^{2+}$  may be operative only at nanometric distances (*i.e.* electron tunnelling distance  $\sim 1\text{--}2 \text{ nm}$ ) which are impossible to resolve with classic optics. The micrometric extension of the ECL region observed herein with TPrA is consistent with the “revisited” route involving both TPrA radicals:<sup>19</sup>



where  $\text{Im}^+$  is the iminium product.

$\text{Ru}(\text{bpy})_3^{2+}$  is not oxidized directly at the electrode in this route. The oxidation of deprotonated TPrA generates the cation radical  $\text{TPrA}^{\bullet+}$  (reaction 2); it deprotonates rapidly to form locally the free radical  $\text{TPrA}^\bullet$ ,<sup>19</sup> which is a strong reductant (reaction 3). This radical reduces  $\text{Ru}(\text{bpy})_3^{2+}$  to  $\text{Ru}(\text{bpy})_3^{\dagger}$  (reaction 4). Then  $\text{TPrA}^{\bullet+}$  oxidizes  $\text{Ru}(\text{bpy})_3^{\dagger}$  to generate the excited state  $\text{Ru}(\text{bpy})_3^{2+*}$  (reaction 5) which deactivates through the emission of a photon. In this path, ECL generation requires the simultaneous presence of both radicals under sufficient fluxes to form the excited state.

Since DBAE is an aliphatic tertiary amine structurally similar to TPrA, it has been proposed to follow mechanisms analogous to TPrA with the formation of radical cation  $\text{DBAE}^{\bullet+}$  and the reducing

intermediate  $\text{DBAE}^\bullet$  by deprotonation.<sup>28–30</sup> Even if DBAE leads to stronger ECL intensity than TPrA when  $\text{Ru}(\text{bpy})_3^{2+}$  is in solution,<sup>7</sup> ECL emission recorded on the modified beads is very low and even undetectable in the side-view configuration. Such an unexpected behaviour might be attributed to the intervention of a much more unstable intermediate (*i.e.* at least 10 times faster deprotonation rate of  $\text{DBAE}^{\bullet+}$ ) which limits drastically the ECL-emitting zone. Our results show the differential reactivity of both model co-reactants and the importance of inspecting the ECL mechanistic pathways with surface-confined species or read/write approaches.

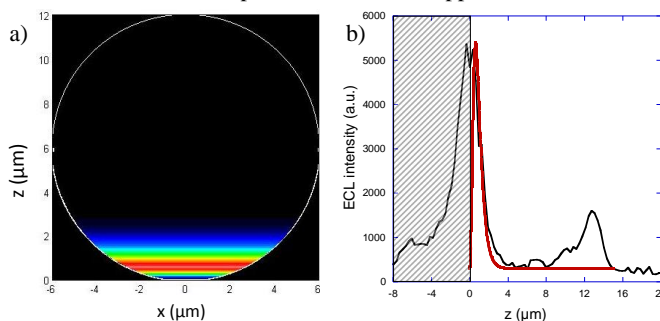


Fig. 4. (a) Side-view of the simulated distribution of the generated  $\text{Ru}(\text{bpy})_3^{2+*}$  excited state (*i.e.* ECL intensity) at the surface of a 12- $\mu\text{m}$  bead. (b) Comparison of the experimental (black line) and simulated (red line) ECL intensity profiles at the level of a single bead. The experimental data correspond to the PS bead of Figure 3a recorded at 1.1 V. The ECL signals are simulated with a value of  $2920 \text{ s}^{-1}$  for the  $\text{TPrA}^{\bullet+}$  deprotonation rate constant. The hatched zone represents the reflection of the ECL light on the electrode surface.

Taking into account the overall mechanistic scheme for TPrA, the concentration profiles of both co-reactant radicals diffusing from the electrode and around the bead were simulated (Figure S3). The spatial location and extension of this ECL-emitting region is also confined in the first 3- $\mu\text{m}$  height of the bead next to the electrode, as evidenced by the simulation (Figure 4a). The ECL profile is constrained by the  $\text{TPA}^{\bullet+}$  and  $\text{TPA}^\bullet$  concentration gradients at the bead surface. Indeed, ECL generation requires the sequential reactions of both reducing and oxidizing TPrA radicals at the same location. Under steady-state, ECL at small  $z$  values reflects the  $\text{TPA}^\bullet$  concentration profile, while the tail of the ECL profile at large  $z$  values mimics the distribution of the most chemically unstable radical (see ESI), here  $\text{TPA}^{\bullet+}$ . The key kinetic parameter in this overall process is the rate constant for the deprotonation of the  $\text{TPrA}^{\bullet+}$ . The position of the maximum ECL intensity and the thickness of this ECL-emitting region depend on the value of this rate constant. If this deprotonation step was slow, then the  $\text{TPrA}^{\bullet+}$  may be formed further away from the electrode and it would result in an extended ECL zone. At the opposite, increasing this reaction rate would contract the ECL zone much closer to the electrode (Figure S4). In particular, the bead confines the different reactive species from hindrance of mass transfer<sup>31,32</sup> allowing for an expansion of the concentration profiles and of ECL-emitting region to greater domains (larger  $z$  values) than those expected from planar diffusion reaction layer conditions (Figure S5).

Figure 4b (black line) shows a typical experimental ECL intensity profile taken along the vertical symmetry axis of a PS bead placed on the GC electrode. The ECL-emitting region is clearly visible and is surrounded by 2 bright zones related to optical effects: the mirror image for  $z < 0$  and the light focused at the top of the bead (*viz.*  $z \sim 13 \mu\text{m}$ ), as discussed previously. We just considered the zone of photon production which contains all information on the chemical

reactivity. The projection of the simulated ECL profile along the same  $z$  symmetry axis is shown on Figure 4b (red line) and the best fit with the experimental data was obtained for a value of  $2920 \text{ s}^{-1}$  for the rate constant of the TPrA $^{\bullet+}$  deprotonation (half-life time of  $\sim 0.24 \text{ ms}$ ). It is in relative good agreement with the value of  $3500 \text{ s}^{-1}$  reported by Miao et al.<sup>19</sup> If the simulated ECL emission profiles fits well with the experimental ones for  $z > 0.6 \mu\text{m}$ , it deviates at the level of the electrode-bead contact ( $z < 0.6 \mu\text{m}$ ). Indeed, the revisited route suggests no TPA $^{\bullet}$  radical at the electrode (then no generation of the luminophore excited state). Experimentally, even if a decrease of intensity was detected for  $z < 0.3 \mu\text{m}$ , the electrode-bead contact region was still illuminated. Eventually, lateral charge propagation between adjacent immobilized ruthenium centres (electron hopping)<sup>33</sup> would extend the light emission toward the bead-electrode interface without affecting the higher  $z$  values (Figure S6). Indeed, for fast surface transformation process,<sup>23</sup> the reactivity at the bead surface is limited by the 3D spatial distribution of the diffusing radical species. The signature of the TPA $^{\bullet+}$  lifetime is then readily obtained from the tail of the ECL distribution.

## Conclusions

In summary, ECL imaging resolved at the single bead level provides a general description of the ECL phenomena operating in bead-based ECL bioassays; it allows deciphering the mechanistic route, testing co-reactant efficiency and showing associated optical focusing effects. Reactivity mapping demonstrates the mechanistic route which leads to ECL emission. Maximum ECL intensity occurs in the micrometric region where concentrations of TPrA $^{\bullet+}$  and TPrA $^{\bullet}$  radicals are locally the highest. Only the luminophores located in the  $3\text{-}\mu\text{m}$  region next to the electrode contribute to the ECL signal and this finite reaction layer defines the optimal size of the functionalized beads for the bioassays. In comparison to bulk situation (*i.e.* freely diffusing Ru(bpy) $_3^{2+}$  in solution), additional thermodynamic and kinetic criteria are required to select efficient co-reactants in the bead-based bioassays: adequate redox potentials and appropriate deprotonation rate constant to form concentrations gradients of both radicals extending simultaneously over sufficiently long distance in order to excite Ru(bpy) $_3^{2+}$ -labels located far from the electrode. We also showed the lens effects of the bead which concentrate the ECL emission and thus contribute to increase the collected analytical signal. Finally, the ECL reactivity imaging offers the opportunity to select new co-reactants with improved sensitivity and to develop new analytical strategies.

## Acknowledgements

We acknowledge helpful discussions with Dr Jérôme Wenger. Financial support has been received from the Ministry of Science and Technological Development (Republic of Serbia) and from the French Foreign Ministry.

## Notes and references

<sup>a</sup> University of Bordeaux, Institut des Sciences Moléculaires, CNRS UMR 5255, ENSCBP, 33607 Pessac, France. E-mail: sojic@enscbp.fr

<sup>b</sup> University of Belgrade, Faculty of Chemistry, 11000 Belgrade, Serbia.

<sup>c</sup> ESPCI ParisTech, PECSA, CNRS UMR 7195, 75231 Paris Cedex 5, France.

Electronic Supplementary Information (ESI) available: Details of experimental procedures and immunoassay. PL and ECL setup and analysis. Simulations. See DOI: 10.1039/b000000x/

- 1 A. J. Bard, *Electrogenerated Chemiluminescence*, M. Dekker, New-York, 2004.
- 2 D. R. Deaver, *Nature*, 1995, **377**, 758-760.
- 3 W. Miao, *Chem. Rev.*, 2008, **108**, 2506-2553.
- 4 J. B. Noffsinger and N. D. Danielson, *Anal. Chem.*, 1987, **59**, 865-868.
- 5 J. K. Leland and M. J. Powell, *J. Electrochem. Soc.*, 1990, **137**, 3127-3131.
- 6 F. Kanoufi, Y. Zu and A. J. Bard, *J. Phys. Chem. B*, 2001, **105**, 210-216.
- 7 X. Liu, L. Shi, W. Niu, H. Li and G. Xu, *Angew. Chem. Int. Ed.*, 2007, **46**, 421 – 424.
- 8 Z. Chen and Y. Zu, *J. Phys. Chem. C*, 2009, **113**, 21877-21882.
- 9 F. Li and Y. Zu, *Anal. Chem.*, 2004, **76**, 1768-1772.
- 10 B. Factor, B. Muegge, S. Workman, E. Bolton, J. Bos and M. M. Richter, *Anal. Chem.*, 2001, **73**, 4621-4624.
- 11 H. Yang, J. K. Leland, D. Yost and R. J. Massey, *Nat. Biotechnol.*, 1994, **12**, 193-194.
- 12 G. F. Blackburn, H. P. Shah, J. H. Kenten, J. Leland, R. A. Kamin, J. Link, J. Peterman, M. J. Powell, A. Shah, D. B. Talley, S. K. Tyagi, E. Wilkins, T.-G. Wu and R. J. Massey, *Clin. Chem.*, 1991, **37**, 1534-1539.
- 13 W. Miao and A. J. Bard, *Anal. Chem.*, 2004, **76**, 5379-5386.
- 14 W. Miao and A. J. Bard, *Anal. Chem.*, 2004, **76**, 7109-7113.
- 15 F. Deiss, C. N. LaFratta, M. Symer, T. M. Blicharz, N. Sojic and D. R. Walt, *J. Am. Chem. Soc.*, 2009, **131**, 6088-6089.
- 16 K. Komori, K. Takada, O. Hatozaki and N. Oyama, *Langmuir*, 2007, **23**, 6446-6452.
- 17 K. Muzyka, *Biosens. Bioelectron.*, 2014, **54**, 393-407.
- 18 Y. Zu and A. J. Bard, *Anal. Chem.*, 2001, **73**, 3960-3964.
- 19 W. Miao, J.-P. Choi and A. J. Bard, *J. Am. Chem. Soc.*, 2002, **124**, 14478-14485.
- 20 S. Wang, E. Harris, J. Shi, A. Chen, S. Parajuli, X. Jing and W. Miao, *Phys. Chem. Chem. Phys.*, 2010, **12**, 10073-10080.
- 21 O. V. Klymenko, I. Svir and C. Amatore, *ChemPhysChem*, 2013, **14**, 2237-2250.
- 22 C. Amatore, B. Fosset, K. M. Maness and R. M. Wightman, *Anal. Chem.*, 1993, **65**, 2311-2316.
- 23 S. Nunige, R. Cornut, H. Hazimeh, F. Hauquier, C. Lefrou, C. Combellas and F. Kanoufi, *Angew. Chem. Int. Ed.*, 2012, **51**, 5208-5212.
- 24 S. O. Krabbenborg, C. Nicosia, P. Chen and J. Huskens, *Nat. Comm.*, 2013, **4**.
- 25 A. Lesch, B. Vaske, F. Meiners, D. Momotenko, F. Cortés-Salazar, H. H. Girault and G. Wittstock, *Angew. Chem. Int. Ed.*, 2012, **51**, 10413-10416.
- 26 H. Aouani, F. Deiss, J. Wenger, P. Ferrand, N. Sojic and H. Rigneault, *Opt. Express*, 2009, **17**, 19085.
- 27 J. Wenger, D. Gérard, H. Aouani and H. Rigneault, *Anal. Chem.*, 2008, **80**, 6800-6804.
- 28 L. Xue, L. Guo, B. Qiu, Z. Lin and G. Chen, *Electrochem. Commun.*, 2009, **11**, 1579-1582.
- 29 S. Wang, J. Milam, A. C. Ohlin, V. H. Rambaran, E. Clark, W. Ward, L. Seymour, W. H. Casey, A. A. Holder and W. Miao, *Anal. Chem.*, 2009, **81**, 4068.

- 30 S. Parveen, W. Zhang, Y. Yuan, L. Hu, M. R. H. Shah Gilani, A. Rehman and G. Xu, *J. Electroanal. Chem.*, 2013, **688**, 45-48.
- 31 E. Suraniti, F. Kanoufi, C. Gosse, X. Zhao, R. Dimova, B. Pouligny and N. Sojic, *Anal. Chem.*, 2013, **85**, 8902-8909.
- 32 S. E. Fosdick, M. J. Anderson, E. G. Nettleton and R. M. Crooks, *J. Am. Chem. Soc.*, 2013, **135**, 5994-5997.
- 33 C. Amatore, Y. Bouret, E. Maisonhaute, J. I. Goldsmith and H. D. Abruña, *Chem. Eur. J.*, 2001, **7**, 2206-2226.

Table of contents:

Mapping the reactivity of a redox-sensitive luminescent microobject positioned in fluxes of reactive species allows analyzing complex mechanistic processes such as the electrogenerated chemiluminescence of model systems used in immunossays.

